Rapid Communications

Approach to the inverse problem of superdiffusion on finite systems based on time-dependent long-range navigation

Alfonso Allen-Perkins,[1,2,*] Alfredo Blanco Serrano,[1,†] Thiago Albuquerque de Assis,[1,2,‡] and Roberto F. S. Andrade[1,3,§]

[1]*Instituto de Física, Universidade Federal da Bahia, 40170-115 Salvador, Brazil*

[2]*Complex System Group, Universidad Politécnica de Madrid, 28040-Madrid, Spain*

[3]*Centre for Data and Knowledge Integration for Health (CIDACS), Instituto Gonçalo Muniz, Fundação Oswaldo Cruz (FIOCRUZ), 41745-715 Salvador, Brazil*

(Received 15 May 2019; published 3 September 2019)

This work addresses the superdiffusive motion of a random walker on a discrete finite-size substrate. It is shown that, with the inclusion of suitably tuned time-dependent probability of large distance jumps over the substrate, the mean square displacement (MSD) of the walker has a power-law dependence on time with a previously chosen exponent $\gamma > 1$. The developed framework provides an exact solution to the inverse problem, i.e., an adequate jump probability function leading to a preestablished solution is evaluated. Using the Markov Chain (MC) formalism, an exact map for the time dependence of the probability function is derived, which depends on the topology of the substrate and on the chosen value of γ. While the formalism imposes no restriction on the substrate, being applicable from ordered Euclidean lattices to complex networks, results for the cycle graph and two-dimensional torus are highlighted. It is also shown that, based on the previously derived probability function, MSD values resulting from direct numerical simulations agree quite well with those solely obtained within the MC framework.

DOI: 10.1103/PhysRevE.100.030101

In real-world complex systems of social, ecological, economic, infrastructural, and technological natures, many dynamical processes occur in discrete spaces, among which are diffusion, agents synchronization, and epidemic spreading [1]. Such systems can be represented by networks in which the nodes and edges indicate, respectively, the entities of the system and the interactions among them. Dynamical processes on these networks usually adopt a nearest-neighbor (NN) strategy of transferring "information" from one node to another. Random-walk models have widespread use both in the analysis of diffusion and navigability in networks, as in exploring their structures to detect their fine-grained organization [2–4].

Currently, it is well documented that there are dynamical processes, both in discrete and continuous spaces, which do not follow this "NN paradigm." For instance, self-diffusive processes of atoms and molecules adsorbed on metals include significant contributions from jumps spanning more distant sites on the metallic surface [5–8]. In the continuum space, the use of random Lévy flights and Lévy walks is widely documented in modeling a variety of processes in which long-range jumps occur together with short-range ones, as in the foraging of species in a given environment [9–13]. Several theoretical approaches have been used to describe such processes as nonlinear diffusion equations [14] or fractional differential equations [15,16] in the continuous space, while fractional transport has also been implemented in networks [17]. More recently, an elegant mathematical approach emerged as an alternative to study dynamical processes on discrete spaces, in which NN and long-distance hops are combined. It is based on the Mellin-transformed d-path Laplacian operator, corresponding to a generalization of the Laplacian operator on graphs [18–21]. Indeed, the so-called long-range interaction (LRI) operator adequately accounts for the effect of jump probabilities that decay with distance. Despite the analytical evidence that continuous time superdiffusion can be induced on continuous and discrete infinite linear substrates by using Lévy flights [15] and Mellin LRIs (MLRIs) [20], respectively, the discrete time behavior on finite complex networks or periodic substrates remains unclear.

The main purpose of this work is to address and advance beyond the mentioned framework, showing that *time-dependent* LRIs (or equivalently long-range navigation or jumps, following, respectively, [22] and [20]) can lead to superdiffusive behavior on finite substrates. This step forward was motivated by our findings that, while the addition of MLRIs on NN cycle graphs actually enhances the speed of the diffusive motion, the mean square displacement (MSD $\equiv \langle r^2(t)\rangle$) traveled by the walker still increases linearly with time. Thus, it is similar to the asymptotic behavior of truncated Lévy flights on the continuous infinite linear substrate [23,24], and to that of continuous time Lévy walks in finite systems [25]. In contrast to previous studies, where the moving particle follows fixed laws for short- and long-range hops, here we consider time-dependent laws, which substantially increase the likelihood of new emergent behaviors. Rather than being a simple mathematical digression, this problem may appear in social or biological systems where agents are

*alfonso.allen.perkins@gmail.com
†alfredoblancoserrano@gmail.com
‡thiagoaa@ufba.br
§randrade@ufba.br

not only influenced by their direct acquaintances but also by certain indirect peer pressure (i.e., LRIs). We can identify three possible scenarios: (i) LRIs remain constant in time; (ii) LRIs decay with time; and (iii) LRIs increase with time. The first situation is the typical one treated in the literature. Instead, the second and the third scenarios are new and may correspond to the decay of fashions and their emergence, respectively. An example of the former can be the case of smoking in Europe and the USA in the early 2000s, whereas the latter can be exemplified by the "binge drinking" [26].

The developed framework is based on Markov chain (MC) formalism. The used strategy consists in solving the inverse superdiffusion problem on discrete time and space: we estimate the time evolution of the MLRI strength, i.e., the time evolution of the Lévy random-walks exponent $\alpha(t)$, which leads to a superdiffusive behavior ($\langle r^2(t)\rangle \sim t^\gamma$) for a preselected value $\gamma > 1$. Although the general framework can be used in any network topology, for the sake of a clearer exposition of our procedure, in this work we consider two Euclidean systems, namely, the cycle graph and the two-dimensional torus (i.e., a square lattice with periodic boundary conditions). This choice guarantees that the saturation effect, present in any finite system, takes place after a sufficiently large time lapse, so that the role played by time-dependent LRIs can be emphasized. Most complex networks, like those generated within the Erdős-Rényi [27] and Barabási-Albert frameworks [28], are characterized by a short diameter, which favors saturation in a short timescale. This requires huge systems in order to precisely characterize superdiffusive behavior. On the other hand, in the case of cycle graphs, exact analytical expressions were derived to estimate $\alpha(t)$ for MLRI walks on these systems. Indeed, for constant α's, they provide the exact evolution of $\langle r^2(t)\rangle \sim t$. For more complex substrates, such as tori, the time evolution of $\alpha(t)$ can also be easily obtained by straightforward numerical evaluation. To draw comparisons to the one-dimensional system, results for walks on tori are also reported.

For the sake of definitiveness, the *discrete time random walk* on a graph is a random sequence of vertices generated as follows: given a starting vertex i, the origin of the walk, at each discrete time step t, the walker jumps with equal probability to one of the NN nodes of its current place [4,29,30]. In the MLRI walk, the walker has a distance depending probability of long-distance jumps. $\langle r^2(t)\rangle$ is a measure of the ensemble average distance between the position of a walker at a time t, and the origin. The behavior $\langle r^2(t)\rangle \sim t^\gamma$ identifies, respectively, normal ($\gamma = 1$), sub- ($\gamma < 1$), or super- ($\gamma > 1$) diffusion. Although $\langle r^2(t)\rangle$ is just one of the measures used to analyze general stochastic data [31,32], it is essential to provide a clear characterization of the diffusive behavior.

From now on, we assume $G = (V, E)$ is a simple, undirected and connected graph with N nodes, without self-loops, described by its adjacency matrix $\mathbf{A}$ with elements $\mathbf{A}(i, j) = \mathbf{A}(j, i) = 1$ if vertices i and j are connected, and $\mathbf{A}(i, j) = 0$ otherwise. Given any pair (i, j), $i \neq j$, $1 \leqslant d_{ij} \leqslant d_{\max}$ represents the shortest path distance between i and j, i.e., the smallest number of edges connecting the nodes i and j. $d_{\max}$, the maximum shortest path distance in the graph, is called the graph diameter. The square, symmetric, $N \times N$, d-path adjacency matrix of G [21] (or neighborhood matrix of order d [33]), is defined by $(\mathbf{A}_d)_{ij} = 1$, if $d_{ij} = d$, and 0 otherwise.

Following [21], let us now consider the Mellin transformed d-path adjacency matrices of G, defined by

$$\hat{\mathbf{A}} = \sum_{d=1}^{d_{\max}} d^{-\alpha}\mathbf{A}_d, \tag{1}$$

where $\alpha \geqslant 0$. Setting $\alpha = -1$, we recover the neighborhood matrix $\hat{\mathbf{M}}$ [33]. If α depends on time [$\alpha \to \alpha(t)$], so will be the transformed d-path adjacency matrices, $\hat{\mathbf{A}} \to \hat{\mathbf{A}}(t)$. We define the strength of a given node i of a transformed d-path graph, at time t, by

$$\hat{s}_t(i) = (\hat{\mathbf{A}}_t\vec{1})_i = \sum_{h\neq i} d_{ih}^{-\alpha(t)}, \tag{2}$$

where $\vec{x}$ is an all-x vector. Note that, in the case of $\alpha(t) \to \infty$, $\hat{s}_t(i) \to k_i$, where $k_i = \sum_{h\in V}\mathbf{A}(i, h)$ denotes the degree of node i. The probability that at time t, a particle sitting on node i hops to $j \neq i$, is defined by

$$P_t(i, j) = \frac{\hat{\mathbf{A}}_t(i, j)}{\hat{s}_t(i)} = \frac{d_{ij}^{-\alpha(t)}}{\sum_{h\neq i} d_{ih}^{-\alpha(t)}}. \tag{3}$$

The transition probability $P_t(i, j)$ defines a dynamical process where the walker can visit the direct neighbors of node i, as well as other nodes that are far away from it. When $\alpha(t) \to \infty$, only NN transitions of a normal random walk are allowed, i.e., $P_t(i, j) = \mathbf{A}(i, j)/k_i$. On the other hand, when $\alpha(t) = 0$, the walker can hop to any other node with equal probability $P_t(i, j) = (1 - \delta_{ij})/(N - 1)$, where δ_{ij} is the Kronecker delta. Finally, in the case of constant α, $P_t(i, j)$ coincides with the transition probability of the Lévy random walk [22,34].

Let us denote by $\hat{\mathcal{S}}_t$ the diagonal matrix with $\hat{\mathcal{S}}_t(i, i) = \hat{s}_t(i)$ and let us define the *transition stochastic matrix* for the random walk, at time t, as $\mathcal{P}_t = (\hat{\mathcal{S}}_t)^{-1}\hat{\mathbf{A}}_t$.

We denote by $\vec{p}_{t,i}$ the vector containing the probability of finding a random walker at a given node of the graph at time t, when the random walker was initially located at node i. Its time evolution is described by

$$\vec{p}_{t+1,i} = \mathcal{P}_t^T\vec{p}_{t,i}, \tag{4}$$

where $\mathbf{X}^T$ stands for the transpose of matrix $\mathbf{X}$. Therefore, it is possible to write

$$\vec{p}_{t,i} = \mathcal{P}_{t-1}^T\cdots\mathcal{P}_0^T\vec{p}_{0,i} = \left(\prod_{\kappa=0}^{t-1}\mathcal{P}_\kappa^T\right)\vec{p}_{0,i}, \tag{5}$$

where $(\vec{p}_{0,i})_j = \delta_{ij}$. If α is constant, $\mathcal{P}_t = \mathcal{P}$, and the MC formulation proposed in Refs. [21,22,35] is recovered.

With the help of Eq. (5), it is possible to quantify the mean distance r covered by a typical walker. Given G and $\vec{p}_{0,i}$, at each time step, we evaluate $r^2(t, i)$ with respect to the origin (node i) as

$$r^2(t, i) = \sum_{j=1}^{N}(d_{ij})^2(\vec{p}_{t,i})_j. \tag{6}$$

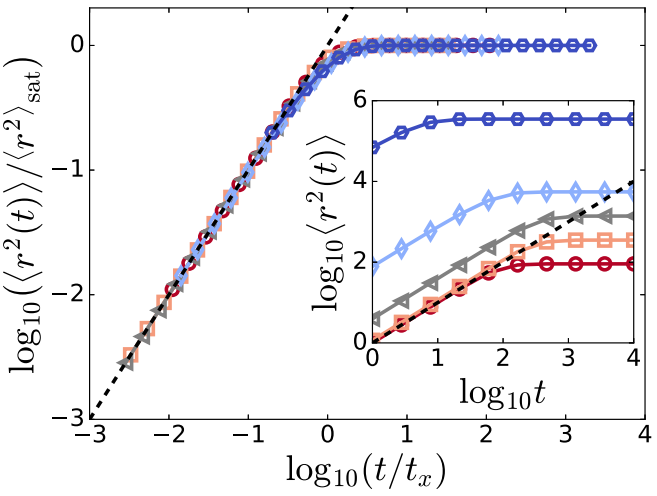

FIG. 1. Collapse of $\langle r^2(t)\rangle$ for various cycle graphs with constant LRIs, by rescalling the curves in the inset with Eq. (12) and $\langle r^2(1)\rangle t_x^\gamma = (N^2-1)/12$, when $\gamma = 1$: $N = 33$ and $\alpha = \infty$ (red circles), $N = 65$ and $\alpha = 5$ (orange squares), $N = 129$ and $\alpha = 3$ (gray triangles), $N = 257$ and $\alpha = 2$ (cyan diamonds), and $N = 2049$ and $\alpha = 1$ (blue hexagons). The black dashed line indicates $f(x) = x$.

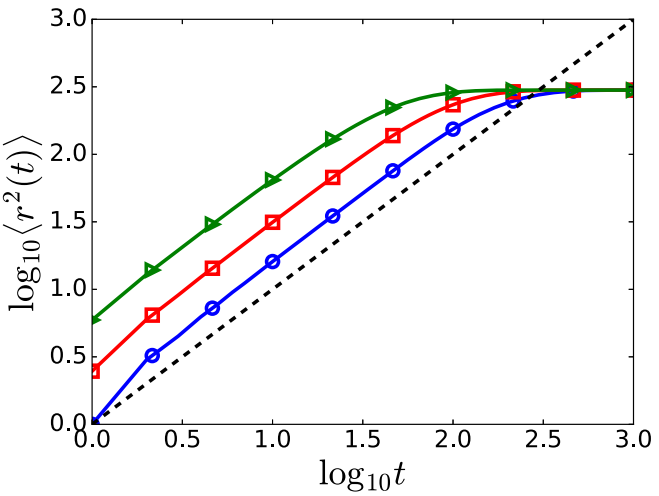

FIG. 2. MC time evolution of $\langle r^2(t)\rangle$ on $N \times N$ tori with constant LRIs: $\alpha = \infty$ (blue circles), $\alpha = 4.2$ (red squares), and $\alpha = 3.5$ (green triangles). The black dashed line is a guide for the eye to locate a normal diffusion.

To obtain numerical estimates for $\langle r^2(t)\rangle$, we average over all the different initial positions of the walker:

$$\langle r^2(t)\rangle = \frac{1}{N}\sum_{i=1}^{N} r^2(t,i) = \frac{1}{N}\sum_{i=1}^{N}\sum_{j=1}^{N}(d_{ij})^2(\vec{p}_{t,i})_j. \quad (7)$$

According to Eqs. (5) and (7), $\langle r^2(t)\rangle$ only depends on the discrete time step t, the weight of the Mellin transformation α, and the topology of $G \leftrightarrow \mathbf{A}$. When MLRI also depends on time, $\langle r^2(t)\rangle$ is also conditioned by the time evolution of $\alpha(t)$. For the finite-size systems considered here, $\langle r^2(t)\rangle$ converges to a saturation value $\langle r^2\rangle_{\rm sat}$ after a characteristic saturation time t_x.

Results obtained from the above equations show that neither constant α's nor arbitrary time-dependent $\alpha(t)$'s lead to well-characterized superdiffusive behavior before saturation. For instance, in Figs. 1 and 2 we show several examples for one-dimensional and two-dimensional (2D) periodic (finite) substrates with constant LRIs, respectively. As can be observed, clearly MLRIs speed up the diffusion of random walkers in these ordered Euclidean lattices. However, normal diffusion persists ($\langle r^2(t)\rangle \sim t$), before saturation appears. Therefore, we now show how to find a precise time evolution of $\alpha(t)$ which, for $t < t_x$, leads to a well-defined superdiffusive behavior. The key step is to look for solutions of the walk satisfying $\langle r^2(t)\rangle = \langle r^2(1)\rangle t^\gamma$. Combining Eqs. (5) and (7) we obtain

$$\langle r^2(1)\rangle t^\gamma = \frac{1}{N}\sum_{i=1}^{N}\sum_{j=1}^{N}(d_{ij})^2\left(\left[\prod_{\kappa=0}^{t-1}\mathcal{P}_\kappa^T\right]\vec{p}_{0,i}\right)_j, \quad (8)$$

which holds for $1 \leqslant t \leqslant \lfloor t_x \rfloor$. Henceforth we consider always $\alpha_0 = \alpha(t=0) = \infty \Rightarrow \langle r^2(1)\rangle = 1$, and $t_x = \langle r^2\rangle_{\rm sat}^{1/\gamma}$ where $\langle r^2\rangle_{\rm sat}$ represents also the squared minimum distance between a pair of nodes, which can be written as

$$\langle r^2\rangle_{\rm sat} = \frac{1}{N^2}\sum_{i=1}^{N}\sum_{j=1}^{N}(\hat{\mathbf{M}}\circ\hat{\mathbf{M}})_{ij}, \quad (9)$$

where $\circ$ represents the Hadamard product. If we consider the particular case $t = 2$, Eq. (8) becomes an implicit equation for $\alpha(t=1)$, once $P_t(i,j)$ in Eq. (3) depends on $\alpha(t)$. The same procedure can now be applied to all subsequent integer values of t, providing a recursive map for the evaluation of $\alpha(t)$. Note that its value depends on all the previous values $\alpha(t')$, with $0 \leqslant t' < t$. Therefore, for any choice of γ and α_0, Eq. (8) leads to a single time evolution $\langle r^2(t)\rangle = \langle r^2(1)\rangle t^\gamma$ and a unique solution $\alpha(t)$.

For the cycle graph, we take advantage of the fact that its transition matrix is circulant. This leads to exact expressions for $\langle r^2(t)\rangle$ even for time-dependent α which, for an odd number of nodes, can be written as (see [36])

$$\langle r^2(t)\rangle = \frac{N^2-1}{12} + \sum_{k=2}^{(N+1)/2}\frac{(-1)^{k+1}}{\sin\left(\frac{\theta_k}{2}\right)}\cot\left(\frac{\theta_k}{2}\right)\mathcal{D}_{t-1}(k), \quad (10)$$

where

$$\mathcal{D}_{t-1}(k) = \prod_{\kappa=0}^{t-1}\left(2H_{0,\frac{N-1}{2}}^{(\alpha_\kappa)}\right)^{-1}\left[\sum_{d=1}^{(N-1)/2}\frac{2}{d^{\alpha_\kappa}}\cos(\theta_k d)\right], \quad (11)$$

$\theta_k \equiv 2\pi(k-1)/N$, $H_{c,n}^{(m)} = \sum_{k=1}^{n}\frac{1}{(c+k)^m}$ is the generalized harmonic number for non-negative n, complex order m, and complex offset c [37]. These expressions were used to evaluate $\langle r^2(t)\rangle$ for several arbitrary sequences of $\alpha(t)$, confirming that (i) if $\alpha(t+1) > \alpha(t)$ [$\alpha(t+1) < \alpha(t)$], diffusion at time $t+1$ becomes slower (faster) than that at time t; and (ii) arbitrary choices of $\alpha(t)$ do not lead to superdiffusion. However, after requiring $\langle r^2(t)\rangle = \langle r^2(1)\rangle t^\gamma$ as in Eq. (8), proper values of $\alpha(t)$ for superdiffusive behavior are obtained for $1 \leqslant t \leqslant$

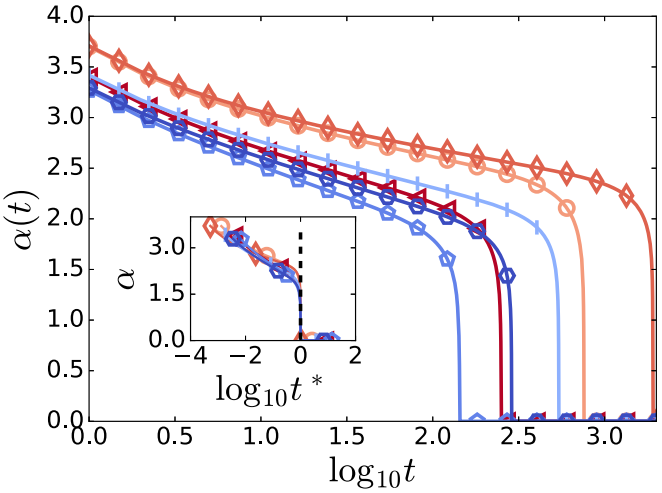

FIG. 3. Time evolution of $\alpha(t)$ for superdiffusive behavior on cycle graphs. $\gamma = 1.5$ and $N = 501$ (circles), and $N = 1001$ (diamonds). $\gamma = 1.8$ and $N = 501$ (triangles), and $N = 1001$ (bars). $\gamma = 2.0$ and $N = 501$ (pentagons), and $N = 1001$ (hexagons). The inset shows α when the X axis is normalized with respect to t_x. The black dashed line indicates $t^* \equiv t/t_x = 1$.

$\lfloor t_x \rfloor$, where $t_x = [(N^2-1)/12]^{1/\gamma}$, $\langle r^2(t)\rangle_{\rm sat} = t_x^{\gamma}$, and

$$\langle r^2(1)\rangle = (-1)^{\alpha_0-2}\frac{H^{(\alpha_0-2)}_{-[(N+1)/2],(N-1)/2}}{H^{(\alpha_0)}_{0,(N-1)/2}}. \tag{12}$$

In Fig. 3 we present the time evolution of $\alpha(t)$ for cycle graphs with different values of N and γ. As anticipated, $\alpha(t)$ is a decreasing function of t, albeit they do not seem to follow any simple dependence on t, e.g., linear, exponential, or power law with a finite cutoff. For a given N, the larger the value of γ, the smaller the values of both t_x and α_1. The diffusion speed increases with γ, and so does the probability of finding the walker far away from the origin. For that reason, $\alpha(t)$ decreases when N is fixed and γ increases. On the other hand, for a fixed γ, the values of t_x and α_1 increase with N, once a larger amount of nodes are far away from the origin. Consequently, the squared minimum distance between a pair of nodes (i.e., $\langle r^2\rangle_{\rm sat}$) also increases. On the other hand, the probability of reaching nodes that are more distant from the origin than those of smaller cycles implies that a weaker MLRI is needed to obtain the same value of $\langle r^2(2)\rangle$. The inset of Fig. 3 shows that there is a smooth cutoff for $\alpha(t)$ when $t^* \equiv t/t_x \approx 1$. Additionally, note that $\alpha(1) > 3$ if $\alpha_0 = \infty$. An exact demonstration of this result when $N \to \infty$ is presented in [36].

Figure 4 shows the MC time evolution of $\langle r^2(t)\rangle$ for all $\alpha(t)$ series in Fig. 3, clearly showing that time-dependent MLRIs induce superdiffusion in the cycle graphs. Such behavior is preserved for t_x time steps until $t^* \lesssim 1$. The smooth cutoff for $\alpha(t)$ takes place to compensate the finite size effects that appear while $\langle r^2(t)\rangle \leqslant \langle r^2\rangle_{\rm sat}$. The superdiffusive phase increases (decreases) with respect to N (γ). For the sake of comparison, results for constant α's are also displayed (see Fig. 1), indicating normal diffusion ($\gamma = 1$). Note the sharp (mild) convergence of $\langle r^2(t)\rangle \to \langle r^2(t)\rangle_{\rm sat}$ when $\gamma > 1$ ($\gamma = 1$).

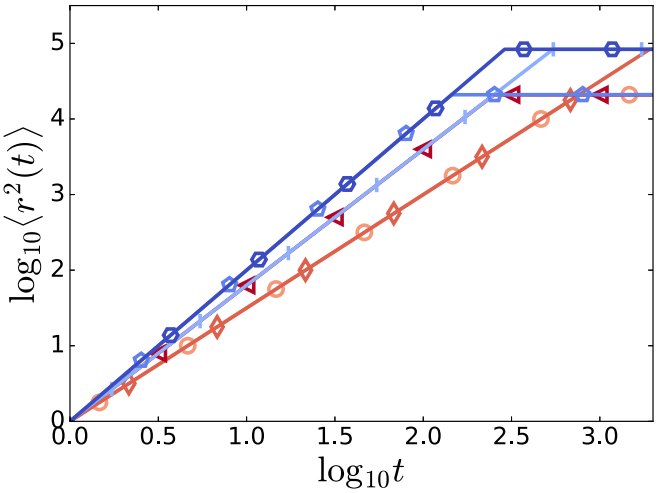

FIG. 4. MC time evolution of $\langle r^2(t)\rangle$ for the series in Fig. 3. $\gamma = 1.5$ and $N = 501$ (circles), and $N = 1001$ (diamonds). $\gamma = 1.8$ and $N = 501$ (triangles), and $N = 1001$ (bars). $\gamma = 2.0$ and $N = 501$ (pentagons), and $N = 1001$ (hexagons).

To validate the adequacy of the procedure to generate superdiffusion, in Fig. 5 we illustrate the time evolution of $\langle r^2(t)\rangle$ obtained from computer simulations for a MLRI cycle graph in which we make use of $\alpha(t)$ obtained within the MC framework. Average results over 5 00 000 independent random realizations are in very good agreement with those obtained when working exclusively within the MC framework.

Results were also obtained for a 2D square lattice with periodic boundary conditions (2D torus). Here, however, as the transition matrices for tori are not circulant, similar expressions to Eqs. (10) and (11) cannot be obtained. Nevertheless, the inverse problem of superdiffusion can be adequately addressed by numerically estimating the solution for $\alpha(t)$ based only on Eq. (8).

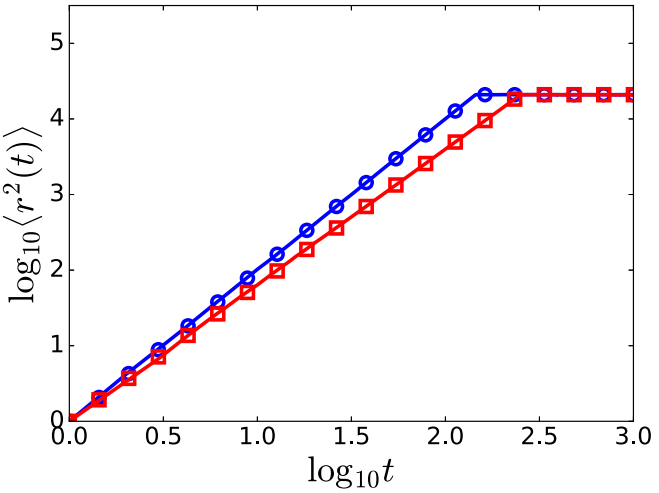

FIG. 5. Time evolution of $\langle r^2(t)\rangle$ on cycle graphs with time-dependent LRIs (i.e., α) obtained by MC (symbols) and numerical simulations (lines) for $N = 501$, when $\gamma = 1.8$ (red squares) and $\gamma = 2.0$ (blue circles).

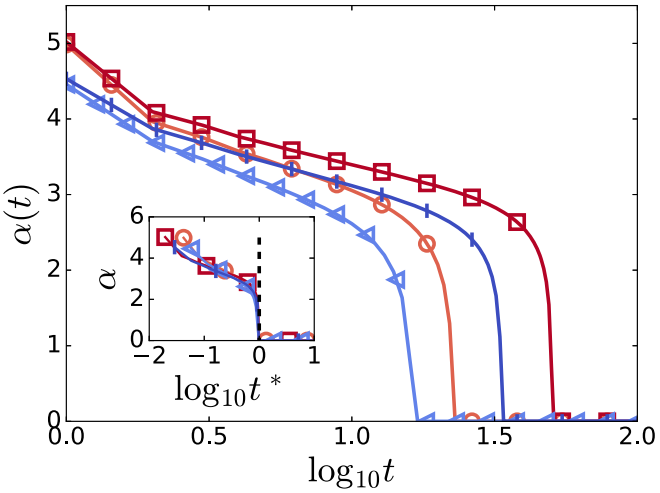

FIG. 6. Time evolution of $\alpha(t)$ for superdiffusive behavior on $N \times N$ tori. $\gamma = 1.8$ and $N = 32$ (circles), $N = 64$ (squares). $\gamma = 2.0$ and $N = 32$ (triangles), $N = 64$ (bars). The inset shows α when the X axis is normalized with respect to t_x. The black dashed line indicates $t^* \equiv t/t_x = 1$.

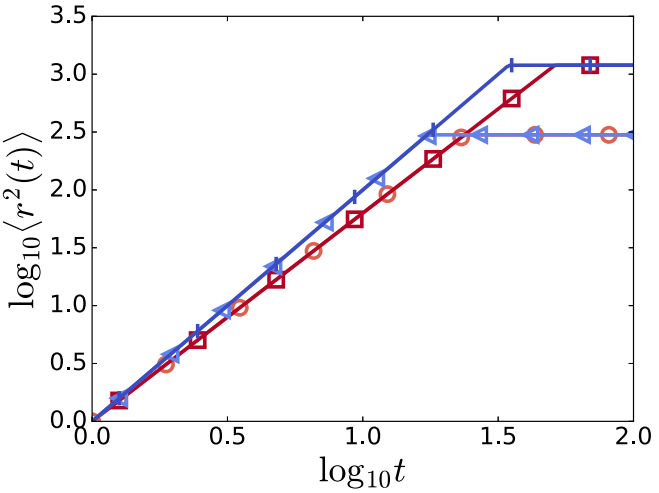

FIG. 7. MC time evolution of $\langle r^2(t)\rangle$ on $N \times N$ tori with time-dependent α. $\gamma = 1.8$ and $N = 32$ (circles), and $N = 64$ (squares). $\gamma = 2.0$ and $N = 32$ (triangles), and $N = 64$ (bars).

In Fig. 6 we show the time evolution of $\alpha(t)$ for tori with different sizes exhibiting superdiffusion ($\gamma = 1.8$ and 2.0). Like it was observed for cycle graphs, for a given γ, the larger the value of N, the larger the values of t_x and α_1. However, in the case of tori, weaker LRIs are needed to induce superdiffusion. This is due to the initial transitory regimen of tori, in which diffusion is faster than that of cycles (see Figs. 1 and 2).

In Fig. 7 we display $\langle r^2(t)\rangle$ for the tori described in Fig. 6. Using the shown $\alpha(t)$, time-dependent LRIs induce superdiffusion on the tori, similarly to what was observed in Fig. 4. Here again, the superdiffusive behavior lasts approximately t_x time steps, during which the smooth cutoff of $\alpha(t)$ compensates the finite size effects present as long as $\langle r^2(t)\rangle \leqslant \langle r^2\rangle_{\text{sat}}$. The duration of the superdiffusive regime can be extended simply by increasing the systems size N, as well as reducing γ. Like circle graphs, results from direct numerical simulations of walks on tori making use of $\alpha(t)$ (not shown) are in best agreement with those in Fig. 7.

Finally, we briefly mention the results of two further random-walk simulations. In first place we considered the effect of replacing $\alpha(t)$ by slightly different, randomly chosen values $\alpha_N(t)$, which might have been caused, for instance, by small changes in the substrate. Working with cycle graphs, our results indicate that $\langle r^2(t)\rangle \sim t^{\gamma+O(X)}$, where $X\alpha(t)$ is the variance of the distribution at time t and $X \to 0$. Next, we asked whether it is possible to obtain a well-defined function $\alpha(t)$ if we require $\langle r^2(t)\rangle$ to follow an arbitrary function $f(t)$. Positive results were obtained when $f(t)$ represents broken power laws. Both traits are illustrated in [36].

This work adds important contributions towards a better understanding of superdiffusive processes on finite discrete substrates, demonstrating how they can be generated by time-dependent navigation. The strategy can be applied to general networks, as well as real case scenarios in which the long-range interactions vary with time. We decided to discuss in detail the Euclidean systems with dimension D, because their diameter $d_{\max}$ and, consequently, saturation time t_x increase according to $\sim N^{1/D}$, making it easier to clearly illustrate the superdiffusive behavior. By contrast, identifying such regime in small-world networks, for which $t_x \sim \log N$, would require one to consider huge values of N. Time-dependent LRIs can be used to develop new navigation strategies, and to improve results for hitting and commute times, among others. On the other hand, given the attention devoted recently to Lévy random walks on multiplex networks, the generalization of this framework to such systems and to weighted or directed networks can be of great interest. Finally, the proposed approach can help explain the known superdiffusive behavior of actual systems using an alternative strategy. Here, covariate models and machine learning methods might identify other node properties capable of generating jump rules similar to the time-dependent α, which differs from the usual approach looking for physical mechanisms to explain the phenomenon.

We gratefully acknowledge J. M. Pastor, E. Estrada, E. Curado, and F. Nobre for fruitful discussions, and the anonymous referees for valuable suggestions. This work was supported by the Brazilian agencies CAPES and CNPq through Grants No. 151466/2018-1 (A.A.-P.), No. 305060/2015-5 (R.F.S.A.), and No. 308343/2017-4 (T.A.A.). R.F.S.A. acknowledges the support of the National Institute of Science and Technology for Complex Systems (INCT-SC Brazil).

[1] E. Estrada, *The Structure of Complex Networks*, Theory and Applications (Oxford University Press, Oxford, 2012).

[2] J. D. Noh and H. Rieger, Random Walks on Complex Networks, Phys. Rev. Lett. **92**, 118701 (2004).

[3] J. Klafter and I. M. Sokolov, *First Steps in Random Walks: From Tools to Applications* (Oxford University Press, New York, 2011).

[4] N. Masuda, M. A. Porter, and R. Lambiottec, Random walks and diffusion on networks, Phys. Rep. **716**, 1 (2017).

[5] M. Schunack, T. R. Linderoth, F. Rosei, E. Lægsgaard, I. Stensgaard, and F. Besenbacher, Long Jumps in the Surface Diffusion of Large Molecules, Phys. Rev. Lett. **88**, 156102 (2002).

[6] C. Yu, J. Guan, K. Chen, S. Chul Bae, and S. Granick, Single-molecule observation of long jumps in polymer adsorption, ACS Nano **7**, 9735 (2013).

[7] T. Ala-Nissila, R. Ferrando, and S. C. Ying, Collective and single particle diffusion on surfaces, Adv. Phys. **51**, 949 (2002).

[8] R. Guantes, J. L. Vega, and S. Miret-Artés, Chaos and anomalous diffusion of adatoms on solid surfaces, Phys. Rev. B **64**, 245415 (2001).

[9] M. Lomholt, K. Tal, R. Metzler, and K. Joseph, Lévy strategies in intermittent search processes are advantageous, Proc. Natl. Acad. Sci. USA **105**, 11055 (2008).

[10] N. E. Humphries, N. Queiroz, J. R. N. Dyer, N. G. Pade, M. Musyl, K. M. Schaefer, D. W. Fuller, J. M. Brunnschweiler, T. K. Doyle, J. D. R. Houghton, G. C. Hays, C. S. Jones, L. R. Noble, V. J. Wearmouth, E. J. Southall, and D. W. Sims, Environmental context explains Lévy and Brownian movement patterns of marine predators, Nature (London) **465**, 1066 (2010).

[11] C. Song, T. Koren, P. Wang, and A.-L. Barabási, Modelling the scaling properties of human mobility, Nat. Phys. **6**, 818 (2010).

[12] I. Rhee, M. Shin, S. Hong, K. Lee, S. J Kim, and S. Chong, On the Levy-walk nature of human mobility, IEEE/ACM Trans. Netw. (TON) **19**, 630 (2011).

[13] G. M. Viswanathan, M. G. E. da Luz, E. Raposo, and H. E. Stanley, *Physics of Foraging* (Cambridge University Press, New York, 2011).

[14] C. Tsallis, *Introduction to Nonextensive Statistical Mechanics: Approaching a Complex World* (Springer, New York, 2009).

[15] R. Metzler and J. Klafter, The random walk's guide to anomalous diffusion: A fractional dynamics approach, Phys. Rep. **339**, 1 (2000).

[16] O. G. Bakunin, *Chaotic Flows*, Springer Series in Synergetics Vol. 10 (Springer, Berlin/Heidelberg, 2011).

[17] A. P. Riascos and J. L. Mateos, Fractional diffusion on circulant networks: Emergence of dynamical small world, J. Stat. Mech.: Theory Exp. (2015) P07015.

[18] E. Estrada, Path Laplacian matrices: Introduction and application to the analysis of consensus in networks, Linear Algebra Appl. **436**, 3373 (2012).

[19] E. Estrada and E. Vargas-Estrada, How peer pressure shapes consensus, leadership, and innovations in social groups, Sci. Rep. **3**, 2905 (2013).

[20] E. Estrada, E. Hameed, N. Hatano, and M. Langer, Path Laplacian operators and superdiffusive processes on graphs. I. One-dimensional case, Linear Algebra Appl. **523**, 307 (2017).

[21] E. Estrada, J.-C. Delvenne, N. Hatano, J. L. Mateos, R. Metzler, and M. T. Schaub, Random multi-hopper model: Super-fast random walks on graphs, J. Complex Netw. **6**, 382 (2018).

[22] A. P. Riascos and J. L. Mateos, Long-range navigation on complex networks using Lévy random walks, Phys. Rev. E **86**, 056110 (2012).

[23] R. N. Mantegna and H. E. Stanley, Stochastic Process with Ultraslow Convergence to a Gaussian: The Truncated Lévy Flight, Phys. Rev. Lett. **73**, 2946 (1994).

[24] I. Koponen, Analytic approach to the problem of convergence of truncated Lévy flights towards the Gaussian stochastic process, Phys. Rev. E **52**, 1197 (1995).

[25] A. Godec and R. Metzler, Linear response, fluctuation-dissipation, and finite-system-size effects in superdiffusion, Phys. Rev. E **88**, 012116 (2013).

[26] P. Ormerod and G. Wiltshire, 'Binge' drinking in the UK: A social network phenomenon, Mind Soc. **8**, 135 (2009).

[27] P. Erdős and A. Rényi, On random graphs I, Publicationes Mathematicae Debrecen **6**, 290 (1959).

[28] A.-L. Barabási and R. Albert, Emergence of scaling in random networks, Science **286**, 5439 (1999).

[29] D. Aldous and J. A. Fill, Reversible Markov Chains and Random Walks on Graphs, https://www.stat.berkeley.edu/users/aldous/RWG/book.html, 2002.

[30] L. Lovász, *Random Walks on Graphs: A Survey, Combinatorics, Paul Erdős is Eighty* (Bolyai Society Mathematical Studies, Keszthely, Hungary, 1993), Vol. 2, p. 1.

[31] E. Almaas, R. V. Kulkarni, and D. Stroud, Scaling properties of random walks on small-world networks, Phys. Rev. E **68**, 056105 (2003).

[32] L. K. Gallos, Random walk and trapping processes on scale-free networks, Phys. Rev. E **70**, 046116 (2004).

[33] R. F. S. Andrade, J. G. V. Miranda, and T. Petit Lobão, Neighborhood properties of complex networks, Phys. Rev. E **73**, 046101 (2006).

[34] T. Weng, M. Small, J. Zhang, and P. Hui, Lévy walk navigation in complex networks: A distinct relation between optimal transport exponent and network dimension, Sci. Rep. **5**, 17309 (2015).

[35] Z. Zhang, T. Shan, and G. Chen, Random walks on weighted networks, Phys. Rev. E **87**, 012112 (2013).

[36] See Supplemental Material at http://link.aps.org/supplemental/10.1103/PhysRevE.100.030101 for the derivation of cycle graphs' formulas, a study of the robustness of our approach, and the results of the inverse problem for broken power laws.

[37] M. J. Kronenburg, Some generalized harmonic number identities, arXiv:1103.5430v2.